Effect of cellulose-based fillers on vulcanized natural rubber

Flavia Leticia Silva Freitas
Universidade de São Paulo
Carla Almêda Correia
Universidade de São Paulo
Letícia Mota de Oliveira
Universidade de São Paulo
Hélio Ribeiro
Mackenzie Presbyterian University
Ticiane Sanches Valera (tsvalera@usp.br)
Universidade de São Paulo

Research Article

Keywords: cellulose nanocrystal, phosphoric acid hydrolysis, natural rubber compound, vulcanization, mechanical properties

Posted Date: April 13th, 2023

DOI: https://doi.org/10.21203/rs.3.rs-2787511/v1

Additional Declarations: No competing interests reported.

Effect of cellulose-based fillers on vulcanized natural rubber

Flávia L. S. Freitas[1] (ORCID https://orcid.org/0000-0002-8960-6476); Carla A. Correia[1] (ORCID https://orcid.org/0000-0002-4509-6574); Letícia M. Oliveira[1]; Hélio Ribeiro[2] (ORCID https://orcid.org/0000-0001-5489-1927); Ticiane S. Valera[1] (ORCID https://orcid.org/0000-0002-5107-9877)

[1] Department of Metallurgical and Materials Engineering - Polytechnic School - University of São Paulo – USP - Av. Professor Mello Moraes, 2463 - Butantã, São Paulo - SP - CEP 05508-030, Brazil.

[2] Escola de Engenharia, Mackenzie Presbyterian University- Rua da Consolação 896, São Paulo, SP CEP 01302-907, Brazil.

Abstract

Cellulose nanocrystal (CNC) fillers have gained attention in research and industrial applications owing to their excellent properties and environmental bias. They can be added to natural rubber (NR) compounds to enhance properties such as the modulus of elasticity. CNCs can be extracted by different acid methods that promote singular features in interfacial adhesion, according to the type of acid used. This study addresses the feasibility of using cellulose nanoparticles in vulcanized NR composites. For this purpose, two different hydrolysis procedures using sulfuric acid and the less aggressive phosphoric acid were performed. These nanoparticles were then added to different amounts of NR compound. The effects of the CNCs on the vulcanization of the NR compound were evidenced by the formation of a zinc-cellulose-rubber complex, which reduced the optimal vulcanization time and increased the NR compound cure rate, particularly for the samples treated with phosphoric acid. In addition, the formation of this complex structure affected the morphology and mechanical properties of the composites. In particular, the tensile strength, elongation at break, and modulus at 300% of the composites with nanocellulose treated with phosphoric acid increased by 90%, 16%, and 51%, respectively, compared to the NR compound. Furthermore, the higher aspect ratio of the nanocellulose particles, mainly treated with phosphoric acid, favored the filler-matrix adhesion, making them a promising alternative to enhance the mechanical properties of NR compounds.

Key words: cellulose nanocrystal, phosphoric acid hydrolysis, natural rubber compound, vulcanization, mechanical properties

Graphical Abstract

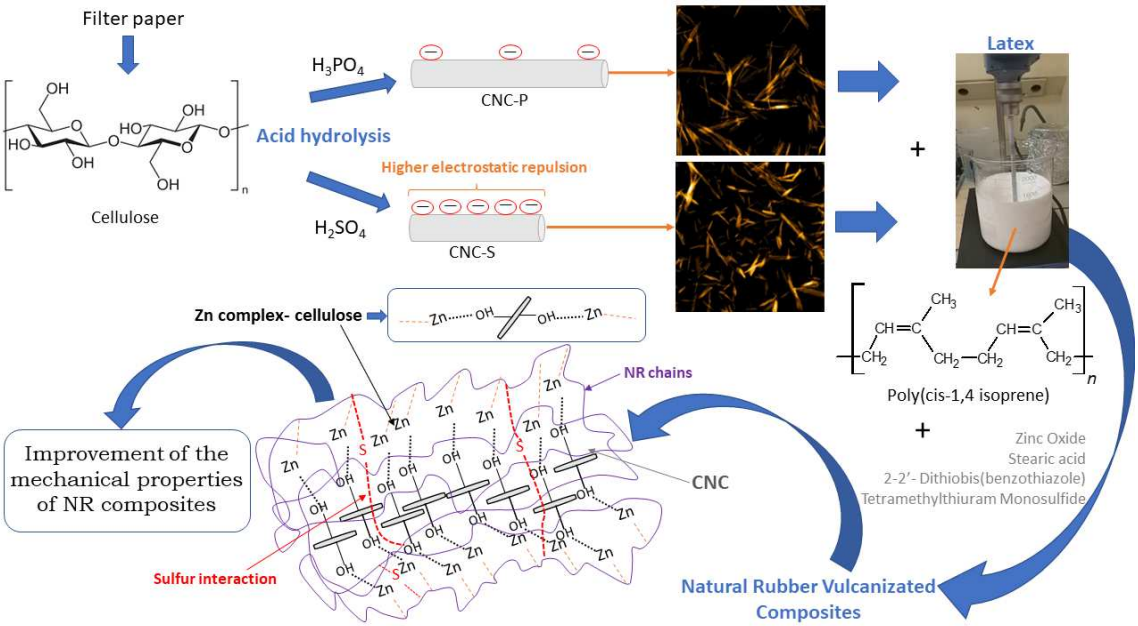

Introduction

Natural rubber (NR) is one of the most important elastomers, used in numerous technological and industrial applications throughout the world. Good processability, high flexibility, outstanding resilience, low hysteresis, and high tear and tensile strengths (strain-induced crystallization) stand out as its main properties (Visakh et al. 2012a, b; Parambath Kanoth et al. 2015). Data from the Association of Natural Rubber Producing Countries (ANRPC) (2021) indicated that around 14 million tons of NR were produced in 2021, corresponding to 48% of the worldwide rubber production. In Brazil, data from the Brazilian Institute of Geography and Statistics (IBGE) reported that the production of NR reached 376.036 tons in 2020 (IBGE, 2020).

Despite the advantages of NR, its low elasticity modulus and abrasion resistance limit its wide applicability. Further enhancement of the mechanical properties of NR can be achieved by reinforcing it with different types of fillers such as carbon black and silica (Martins et al. 2008; Pantamanatsopa et al. 2014; Zhang et al. 2014; Ali et al. 2020), which are among the most commonly used in industrial applications. However, some of these materials are obtained from non-renewable sources and require large amounts of energy for production. For this reason, among others, natural cellulose-based fillers are gaining attention in both research and industrial sectors, in addition to the excellent

specific chemical and physical properties exhibited by such materials. Therefore, the development of low-density and environmentally friendly reinforcement fillers such as cellulose nanocrystals (CNCs) has been identified as a potential replacement for traditional fillers (Tian et al. 2017; Phanthong et al. 2018; Chawalitsakunchai et al. 2019; Dittanet et al. 2019; Lavanya and Natchimuthu 2019; Nie et al. 2019; Tao et al. 2019; Ali et al. 2020).

The cellulose structure, which remains unaltered in the CNC, is formed by the repeated connection of two 1,4-β glycosidic bonds through hydrogen bonds (Habibi et al. 2010; Moon et al. 2011; Kargarzadeh et al. 2018; Wang et al. 2019; Ali et al. 2020). In addition to their renewability, CNCs combine biodegradability, high aspect ratio, flexibility, low density, and high strength. Furthermore, the CNC surface can be tailored to improve its adhesion to polymer matrices when used as a reinforcement agent. The surface treatments of CNCs are generally classified according to the chemical nature of the extraction method used to obtain the nanoparticles (Moon et al. 2011; Phanthong et al. 2018). CNCs can be produced by acid hydrolysis using hydrochloric, hydrobromic, phosphoric, citric, oxalic, maleic, and sulfuric acids. Therefore, different CNC-charged surfaces are produced, depending on the acid used in the hydrolysis (Phanthong et al. 2018; Vanderfleet et al. 2018). Sulfuric acid is the most commonly used, and its high sulfate content provides a highly negatively charged sulfate-ester surface that stabilizes the CNC dispersion and increases the compatibility of the CNC/resin system (Moon et al. 2011; Gan and Chow 2019). However, the presence of charged sulfate groups in a composite may reduce the thermal stability of the matrix (Habibi et al. 2010; Xie et al. 2018).

Orthophosphoric acid synthesis is a promising alternative that produces CNC particles exhibiting enhanced thermal stability and a small amount of surface charges compared with that obtained using sulfuric acid (Camarero Espinosa et al. 2013; Eyley and Thielemans 2014; Lu et al. 2014; Xie et al. 2018; Gan and Chow 2019). However, the ionic repulsion between the charged sulfate groups is known to promote their dispersibility much better than the CNC superficial charges introduced by phosphoric acid hydrolysis (Camarero Espinosa et al. 2013). Nevertheless, stable suspensions can be obtained when anionic phosphate half-ester surface groups are present (Camarero Espinosa et al. 2013). In addition, the authors noted that nanocomposites of ethylene oxide−epichlorohydrin copolymers prepared with CNCs extracted using phosphoric acid

showed a better reinforcing capability than those hydrolyzed using hydrochloric or sulfuric acids.

When added to an elastomeric compound, fillers such as CNCs can significantly improve the mechanical properties of the matrix phase (Siqueira et al. 2011; Zhang et al. 2014; Tian et al. 2017; Dittanet et al. 2019; Nie et al. 2019; Tao et al. 2019). Zhang et al. (Zhang et al. 2014) observed that the NR tensile strength and modulus increased by 38% and 433%, respectively, upon a 5 wt% CNC addition to NR, thereby resulting in a 16% decrease in the elongation at break. Nie et al. (Nie et al. 2019) investigated the application of CNCs in epoxidized NR (ENR). As expected, CNC addition effectively improved the mechanical properties of the nanocomposite, although it reduced the elongation at break with increasing CNC content, probably due to the formation of hydrogen-bonding crosslinked networks, which, in turn, restricted the movement of the ENR molecular chains. Dittanet et. al (Dittanet et al. 2019) reported that the tensile strength, tensile stress at 200% elongation (200% modulus), and elongation at break increased with the addition of CNC to NR. The authors used sulfuric acid-hydrolyzed CNC and observed a 30% increase in the tensile strength for 2 wt% CNC addition.

Numerous studies (Siqueira et al. 2011; Gao et al. 2013; Parambath Kanoth et al. 2015; Chawalitsakunchai et al. 2019; Silva et al. 2019) have been performed using multiple sources of cellulosic nanoparticles for elastomeric reinforcement, and some of them have focused on investigating the properties of unvulcanized NR.

Although the CNC phosphoric acid extraction is already well established, there are no reports on composites that use such CNCs in vulcanized NR extracted from latex. Therefore, in this work, a comparative study was performed on the morphological/structural and mechanical/rheological characteristics of NR composites prepared with CNCs obtained from phosphoric and sulfuric acid hydrolysis. The morphological and structural characteristics of the CNCs were studied using atomic force microscopy (AFM), X-ray diffraction (XRD), X-ray excited photoelectron spectroscopy (XPS), and thermogravimetric analysis (TGA). Moreover, a new approach is proposed to improve the properties of vulcanized NR compounds reinforced with CNC obtained by hydrolysis with the less aggressive phosphoric acid instead of the widely used sulfuric acid. In addition, this research strongly emphasizes the use of bio-based materials obtained from renewable sources.

Experimental

Materials

NR was supplied in a centrifugated latex form by BDF Trade in Agricultural Products of São Paulo, Brazil. CNCs were prepared with the acid hydrolysis method, using a quantitative filter paper (CAAL Ltda., Brazil, ash content of 0.00013 g). Orthophosphoric and sulfuric acids (Labsynth Ltda., Brazil) were used for acid hydrolysis and glacial acetic acid (CAAL Ltda., Brazil) was used for the latex coagulation.

Preparation of CNC

Acid hydrolysis of filter paper (40 g) was performed with a 63 wt% sulfuric acid (H_2SO_4) solution in a ratio of 1:10 (g/ml) at 45 °C for 50 min under continuous agitation. In addition, acid hydrolysis of filter paper (40 g) was performed with a 10.5 M orthophosphoric acid (H_3PO_4) solution in a ratio of 1:20 (g/ml) at 100 °C for 60 min under agitation, using a method similar to that developed by Camarero Espinosa et al. (Camarero Espinosa et al. 2013). The obtained suspensions were quickly cooled, diluted with deionized water to 1000 mL, and centrifuged at 17,000 rpm for 10 min, followed by three centrifugation processes of 5 min each to remove the excess acid present in the suspension. The resultant precipitates were dialyzed against deionized water for 7 days until a constant neutral pH was achieved. The suspensions of CNCs were then dispersed using an Ultraturrax mixer and subsequently by ultrasonic tip treatment for 10 min to prepare CNCs. The CNCs obtained from hydrolysis with sulfuric acid are hereafter referred to as CNC-S, and those with phosphoric acid as CNC-P. For TGA, XRD, and XPS analyses, the CNC-S and CNC-P samples were dried in a vacuum oven at a temperature of 60 °C for 12 h.

Preparation of NR composites

To prepare NR composites, the amount of filler was calculated for final concentrations of 2.5, 5.0, and 10.0 phr of CNCs according to the amount of NR in the latex (60 wt%). The CNC dispersion in each sample was mechanically stirred for 2 h at 300 rpm at room temperature to obtain a homogeneous mixture. The final emulsions were coagulated by the progressive addition of acetic acid solution with a molar concentration

of 3 mol/L. The coagulated rubber was washed with distilled water until a neutral pH was achieved. Subsequently, thin sheets of rubber were dried under vacuum at 60 °C until constant weight was achieved. NR composites with different CNC contents were prepared using a Mecanoplast two-roll mill (model C400 I) with 25 × 34 rpm rotation and 1:1.4 friction. Table 1 shows the formulation of composites in parts per hundred parts of rubber (phr) with different contents of CNCs and unfilled rubber compound.

Table 1 Formulation of the natural rubber (NR) compound and composites

Sample	NR	CNC	Zinc oxide	Stearic acid	MBTS[a]	TMTD[b]	Sulfur
NR	100	0	4	1	1	0.5	1.5
NR + CNC-S or P 2.5	100	2.5	4	1	1	0.5	1.5
NR + CNC-S or P 5	100	5	4	1	1	0.5	1.5
NR + CNC-S or P 10	100	10	4	1	1	0.5	1.5

[a]2-2'- Dithiobis(benzothiazole) [b] Tetramethylthiuram Monosulfide

The formulations of the NR compound and composites (Table 1) were prepared according to (Formela et al. 2016; Moonart and Utara 2019). The components were added sequentially and mixed for 5 min until the compound was completely homogenized. To obtain the cure time for vulcanization (t_{90}), vulcanization curves were obtained using an oscillating disc rheometer ODR 2000 (TEAM, Brazil), according to ASTM D-2084-11. The vulcanization was performed using a hydraulic press machine at a temperature of 160 °C, running time of respective t_{90}, and 20 MPa pressure.

Characterization methods

XRD

The XRD analyses of the filter paper and CNC samples were performed in a Philips XPERT-MPD diffractometer, with Cu Kα radiation (λ = 1.5406 Å), in the 2θ range from 5 to 40º, with steps of 0.02°, and soaking time of 2.5 s. The pristine filter paper was used as purchased, and the CNC samples, dried in a vacuum oven, were ground with a mortar and pistil and sieved through a 325 mesh. The crystallinity index (CI) was estimated by subtracting the amorphous halo (Park, Sunkyu, Baker, John O, Himmel,

Michael E, Parilla, Philip A and Johnson 2010) from the XRD curves, by creating a baseline. The CI was calculated using Equation 1,

$$CI(\%)=\frac{A_c}{A_t} \times 100 \quad (1)$$

where A_t is the total area of the XRD curves, and A_c is the sum of the peak areas corresponding to the cellulose crystalline structure; both A_t and A_c were calculated after the correction baseline.

XPS

XPS analyses were performed using a surface analyzer (Thermo Fisher Scientific) with a monochromated Al-Kα X-ray source (1486.6 eV). A resolution of 1 eV was used for the survey scans. The peaks were deconvoluted using the Avantage software (Thermo Fisher Scientific).

AFM

The CNCs were analyzed with a Bruker microscope using the Peak Force method (Multi mold 8). The images were acquired using ScanAsyst-air probes (silicon tips on a silicon nitride lever) at a scan rate of 1 Hz and 512 × 512-pixel resolution. The nominal spring constant of the cantilever was 0.4 N/m. The aqueous CNC suspensions were diluted with distilled water. The samples were prepared using drops of CNC dilute dispersions (0.1 mg/ml) deposited on mica substrate and dried at 25 °C. The diameter (d), length (L), and aspect ratio (d/L) of the CNC samples were measured for 70 nanocrystals in each CNC sample using Gwyddion Surface Data software.

TGA

The TGAs were performed using a Netzsch-brand equipment (model STA 449). The analyses were performed in triplicate using 10 mg of each sample in alumina crucibles. The samples were heated from room temperature to 1000 °C at a rate of 10 °C / min under a nitrogen atmosphere with 20 ml/min of gas flow. The maximum degradation temperature (T_{max}) and initial temperature of thermal degradation (T_{onset}) were obtained from the derivative thermogravimetric (DTG) curves, with T_{onset} corresponding to the first inflection point of the curves.

SEM-FEG

Specimens of NR and composites were analyzed using SEM-FEG (FEI, INSPECT F50 SEM-FEG model). Micrographs were collected at an accelerating voltage of 15 kV. Energy-dispersive spectroscopy (EDS) was used to analyze the semi-quantitative chemical composition of the unfilled NR compounds and composites. The samples were prepared by cutting with a diamond knife at a cryogenic temperature (-120 °C) in ultramicrotome (Leica, model EM FC6). The surfaces were sputter-coated with a gold protective film (Balzers Sputter Coater).

Mechanical tests

The mechanical properties were measured using an Alpha Technologies universal testing machine (model Tensometer T 2000) equipped with a 1 kN load cell. The experimental procedure was performed with five replicate specimens in accordance with ASTM D412-06. The tests were conducted at room temperature at a testing velocity of 500 mm/min.

Crosslink Density

The crosslink density (ν) values were determined by the swelling method using Equation 2 (Flory and Rehner 1943; Mathew et al. 2001), where *Mc* is the molecular weight between the crosslinks, calculated using Equation 3, v_n is the molar volume of the solvent, ρ_p is the density of the polymer, and V_{rf} is the volume fraction of the rubber phase in the swollen gel of the rubber vulcanizate.

$$\nu = \frac{1}{2M_c} \tag{2}$$

where,

$$M_c = \frac{-\rho_p v_n {V_{rf}}^{1/3}}{[ln(1 - V_{rf}) + V_{rf} + \chi V_{rf}^2]} \tag{3}$$

χ is the interaction parameter between the polymer and solvent and is expressed by Equation 4 (Flory and Rehner 1943; Mathew et al. 2001).

$$\chi = \beta + \frac{v_n}{RT}(\delta_s - \delta_p)^2 \quad (4)$$

where β is the lattice constant; δp and δs are the solubility parameters of the polymer and solvent, respectively; R is the gas constant; and T is the absolute temperature.

V_{rf}, expressed in Equation 5, was calculated by considering only the fraction of the rubber compounds, that is, by subtracting the fiber amount using the empirical density of each filler, as described by Jacob et al. (Jacob et al. 2004).

$$V_{rf} = \frac{(d - fw)\rho_p^{-1}}{(d - fw)\rho_p^{-1} + A_s\rho_s^{-1}} \quad (5)$$

where d is the de-swollen weight of the sample, f is the volume fraction of the fiber, w is the initial weight of the sample, ρ_s is the density of the solvent, and A_s is the amount of solvent absorbed by the sample.

The swelling of the NR compound and composites was performed in toluene for 72 h at room temperature using square samples with a width of 10 mm and a thickness of 2 mm.

Results and discussion

XRD results

Fig. 1 shows the X-ray diffraction curves obtained for the pristine filter paper and the CNCs obtained by hydrolysis with sulfuric acid (CNC-S) and phosphoric acid (CNC-P).

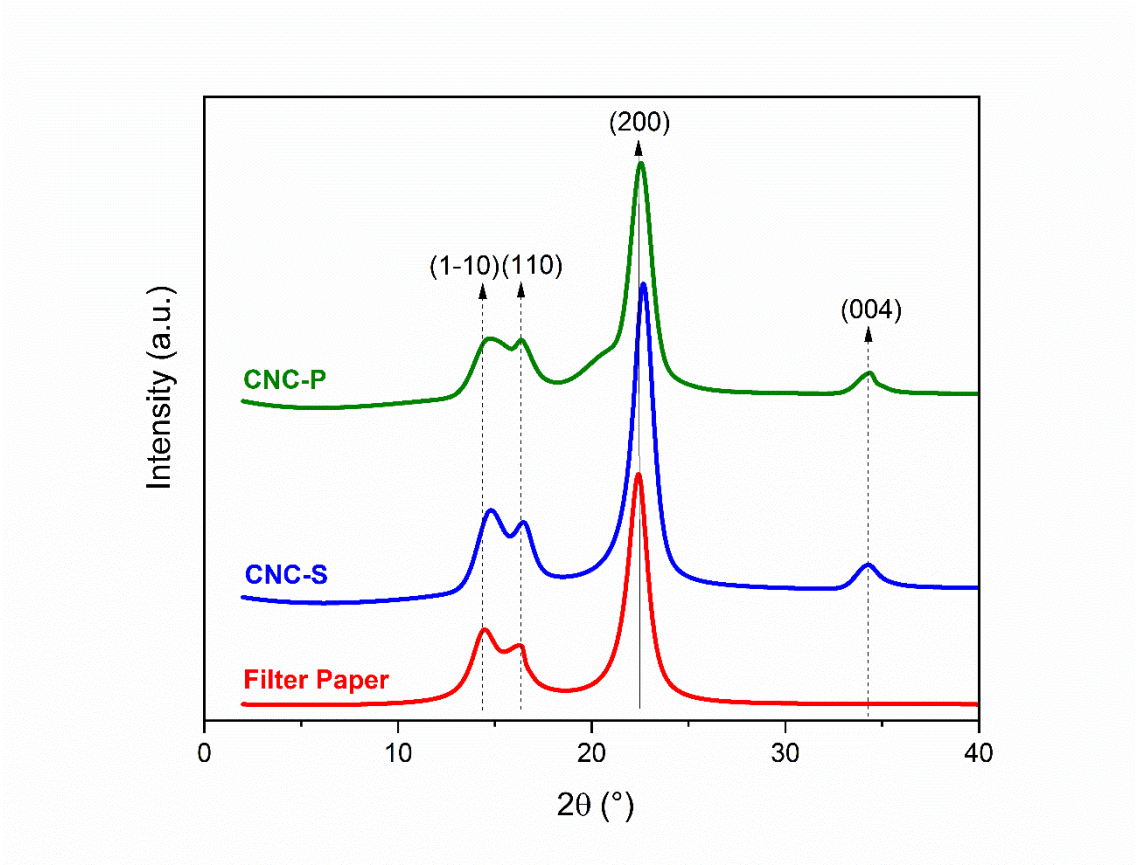

Fig. 1 XRD curves of the pristine filter paper and the CNCs extracted with sulfuric acid (CNC-S) and phosphoric acid (CNC-P)

All the curves presented have the characteristic peaks of cellulose I. The highest intensity peak at approximately 2θ = 22.3° corresponds to the crystallographic plane (200). The lower intensity peaks at approximately 2θ = 14.5 ° and 16.4 correspond to the lattice planes (1-10) and (110), respectively. These peaks are characteristic of cellulose Iβ.

The peak at 2θ = 34,3° is attributed to the (004) plane, and the increase in its intensity indicates a higher crystallinity compared to that of the pristine material (filter paper) (Kasyapi et al. 2013). Thus, the crystallinity index calculated for the filter paper, CNC-S, and CNC-P are 78%, 83% and 80%, respectively. These results indicate the removal of the amorphous regions of cellulose by the treatments performed (Martins et al. 2011; Thomas et al. 2015).

TGA results

The thermal stability of CNCs is a very important characteristic, as vulcanized composites are processed at high temperatures. The TGA curves and their derivatives obtained for the pristine filter paper, CNC-S, and CNC-P are shown in Fig. 2.

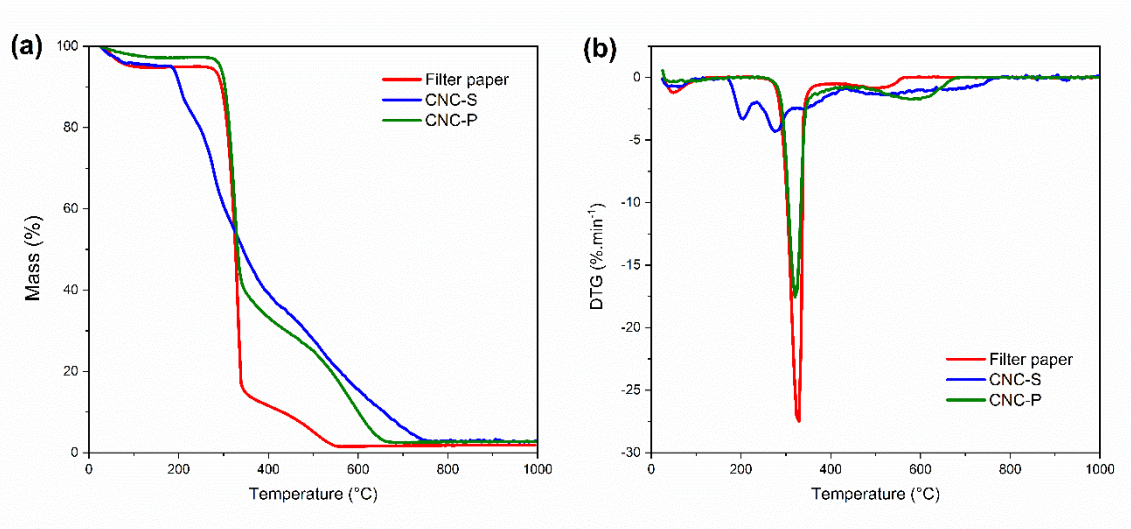

Fig. 2 TGA (**a**) and DTG **(b)** curves of the pristine filter paper, CNC-S, and CNC-P

Figs. 2a and 2b show that the weight loss in all samples occurred in three major steps during the heating ramp. The first occurred between room temperature and approximately 100 °C, and can be attributed to loss of moisture. The loss of water in the filter paper and CNC-S is 5 wt%, and that in CNC-P is approximately 3 wt%.

In the second stage, approximately between 150 and 400 °C, CNC-P and the pristine filter paper present the same degradation behavior that occurred in a single step. These samples exhibit the typical cellulose degradation behavior. At this stage, the degradation starts from the depolymerization step, in addition to the dehydration and decomposition of the glycosidic structure. The CNC-S sample exhibits a complex degradation behavior that occurred in multiple steps (Fig. 2b). In the process of the CNC-S degradation, the hydrolysis of the sulfated cellulose occurred initially and subsequently the decomposition of the amorphous regions in the temperature range 150–300 °C, followed by steps of dehydration and depolymerization that occurred between 300 and 415 °C (Roman and Winter 2004; Camarero Espinosa et al. 2013). The last stage, approximately between the 500 and 750 °C, is related to the degradation of the carbonaceous residues (Shen et al. 2017).

316 Table 2 shows the values of the initial thermal degradation temperature (T_{onset})
317 and maximum degradation temperature (T_{max}) obtained from the DTG curves (Fig. 2b),
318 and the residue content at 500 °C obtained from the TGA curves (Fig. 2a).
319
320 **Table 2** Onset degradation temperature (T_{onset}), maximum degradation temperature
321 (T_{max}), and residues at 500 °C, obtained from the TGA and DTG curves.

Sample	T_{onset} (°C)	T_{max} (°C)	Residues at 500 °C (%)
Pristine filter paper	275	227	5
CNC-S	170	276	28
CNC-P	278	320	25

322
323 CNC-S showed lower thermal stability than CNC-P and the pristine filter paper.
324 This behavior can be attributed to the degradation of cellulose, which can be catalyzed by
325 sulfuric acid (Roman and Winter 2004). The residual mass at 500 °C of CNC-S and CNC-
326 P is higher than that of the filter paper. CNC-S and CNC-P have higher crystallinity than
327 the filter paper, and the energy required to break the intermolecular bonds is higher
328 (Huang et al. 2018).
329
330 AFM results
331
332 Fig. 3 shows AFM images at two different scales for CNC-S and CNC-P.

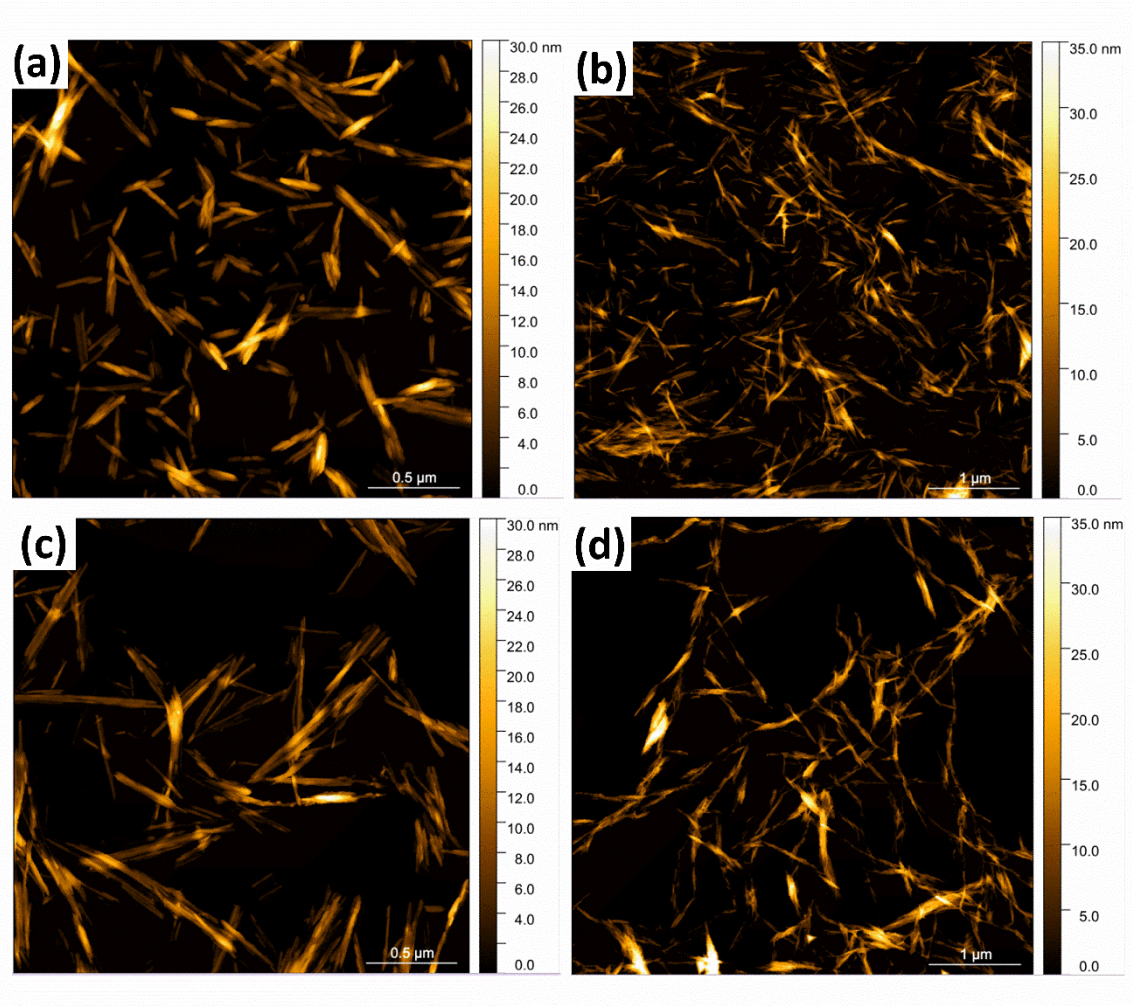

Fig. 3 Topographic AFM images of CNC-S with scan sizes of 2.5 x 2.5 µm **(a)** and 5 x 5 µm **(b)**, and CNC-P with scan sizes of 2.5 x 2.5 µm **(c)** and 5 x 5 µm **(d)**.

Clearly, the structures obtained from both hydrolysis conditions are found at the nanometer scale, and the particles exhibit the shape of a needle. Furthermore, it the nanocrystals tend to interconnect after the drying of the aqueous dispersion, forming agglomerates because of the formation of intermolecular hydrogen bond. Particularly, in the 2.5 x 2.5 µm-scan size AFM images, the CNC-P samples seem to be more agglomerated than the CNC-S ones. This behavior is expected because it is known that CNC-P has a lower density of surface electrostatic charges compared to CNC-S, which has sulfate groups grafted onto its surface (Camarero Espinosa et al. 2013).

The diameter (d) and length (L) were measured to estimate the dimensions of the nanocrystals found individually in the images. The distributions of the diameter, length, and the aspect ratio (AR), are illustrated in Fig. 4.

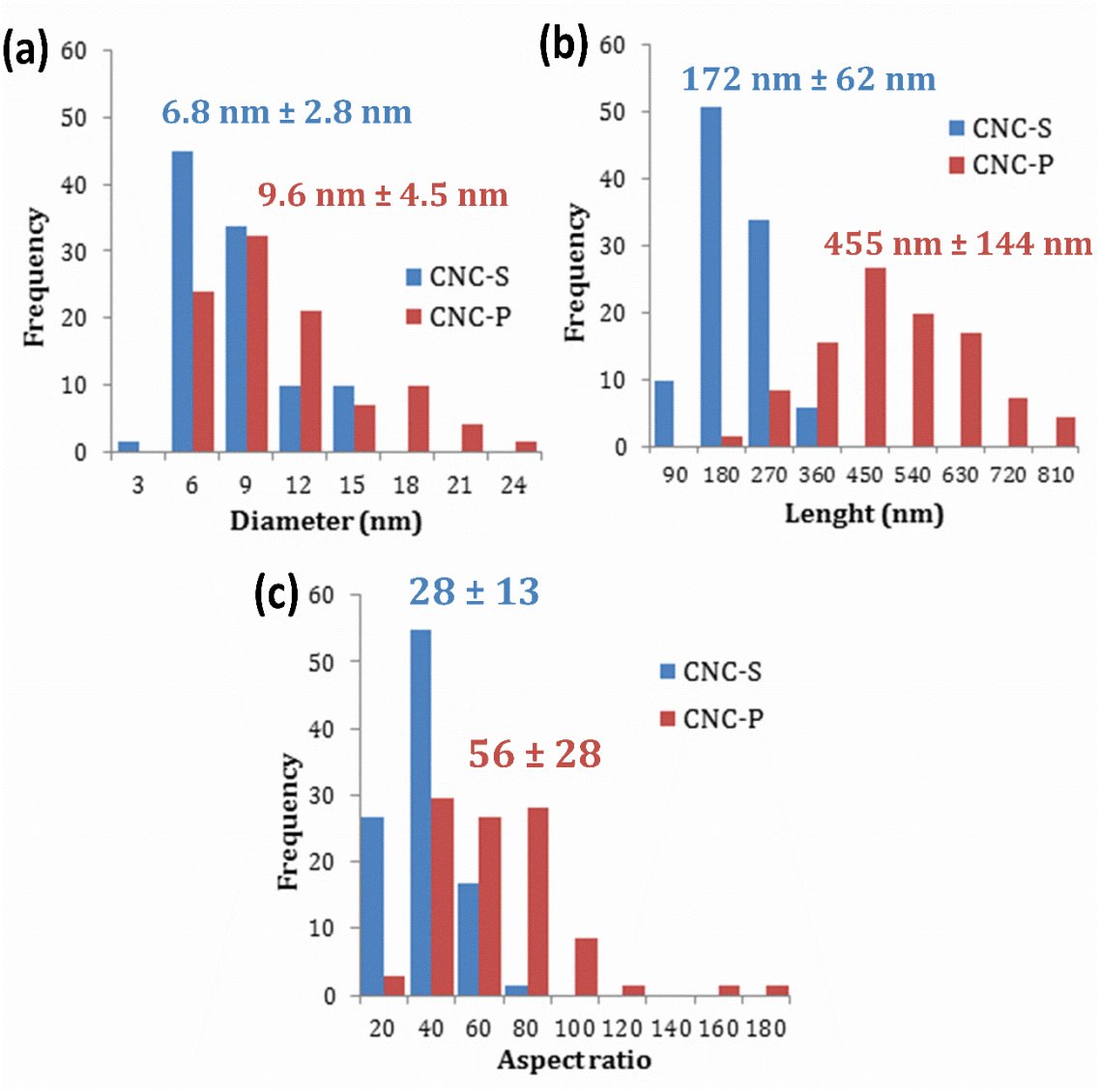

Fig. 4 Distributions of the diameter (a), length (b), and aspect ratio (c) of the CNC-S and the CNC-P samples, measured from AFM images

As shown in Fig. 4, CNC-S has smaller dimensions and a lower aspect ratio than CNC-P. It is possible to observe a slightly wider distribution in the values of the diameter, length, and aspect ratio for CNC-P, indicating that these nanocrystals are more irregular in size than CNC-S. These results do not agree with those reported in the literature (Dufresne 2012).

XPS analysis

Fig. 5 shows the survey photoemission spectra in the region between 0 and 1400 eV of the pristine filter paper, CNC-S, CNS-P.

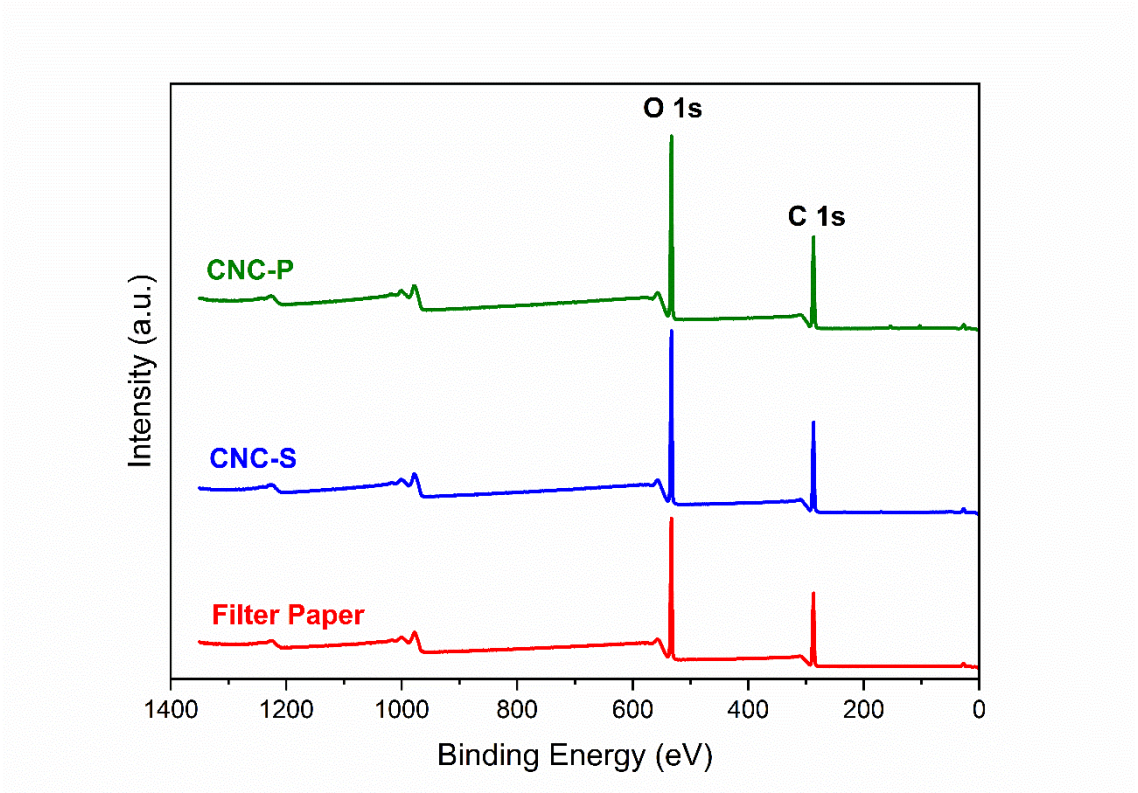

Fig. 5 XPS survey spectra of the pristine filter paper, CNC-S, and CNC-P

Peaks at 533 and 287 eV are observed for all samples and can be attributed to the presence of O1s and C1s, respectively (Ribeiro et al. 2015; Lima et al. 2016). According to the chemical structure of cellulose, formed by D-glucose units $(C_6H_{10}O_5)_n$, the presence of oxygen is mainly related to the hydroxyl groups, which can undergo oxidation and be converted into carboxyl groups, contributing to an increase in the intensity of the normalized O1s peak (Li et al. 2015). Table 3 shows the mass concentrations of the pristine filter paper, CNC-S, and CNC-P. A very small peak attributed to sulfur is observed at approximately 170 eV. However, the phosphorus peak (135 eV) was not detected in the survey spectra.

Table 3 C, O, and S mass concentrations and O/C ratio obtained by the survey spectrum for the pristine filter paper, CNC-P, and CNC-S.

Sample	% O	% C	%S	O/C

Pristine filter paper	42.9 ± 0.4	57.1 ± 0.4	0	0.75
CNC-S	43.5 ± 0.5	56.2 ± 0.5	0.3 ± 0.1	0.76
CNC-P	43.1 ± 0.3	56.9 ± 0.3	0	0.77

For CNC-S, the presence of sulfur on the sample surface (see Table 3) is due to the sulfate groups originating from the acid hydrolysis performed with sulfuric acid (Li et al. 2015). The sulfur concentration (0.3%) corresponds to 1.53 sulfate groups per 100 anhydro glucose units, according to the calculation described by Li et al. (Li et al. 2015). The value achieved for the sulfate groups is in agreement with that reported in CNC studies using sulfuric acid (Li et al. 2015; El Achaby et al. 2018). However, this value is close to the detection limit of the equipment (0.1%). Sulfate groups present on the surface of CNCs create an electrostatic repulsion between them, hindering their agglomeration. The presence of sulfate groups in CNC-S and the absence of phosphate groups in CNC-P explain the AFM images, as there is a greater amount of agglomerates in the nanocrystals extracted by sulfuric acid than in those extracted by phosphoric acid.

Vulcanization characteristics

Fig. 6 shows the rheometric curves obtained for the NR compound and composites with CNC-P (NR + CNC-P) and CNC-S (NR + CNC-S) additions.

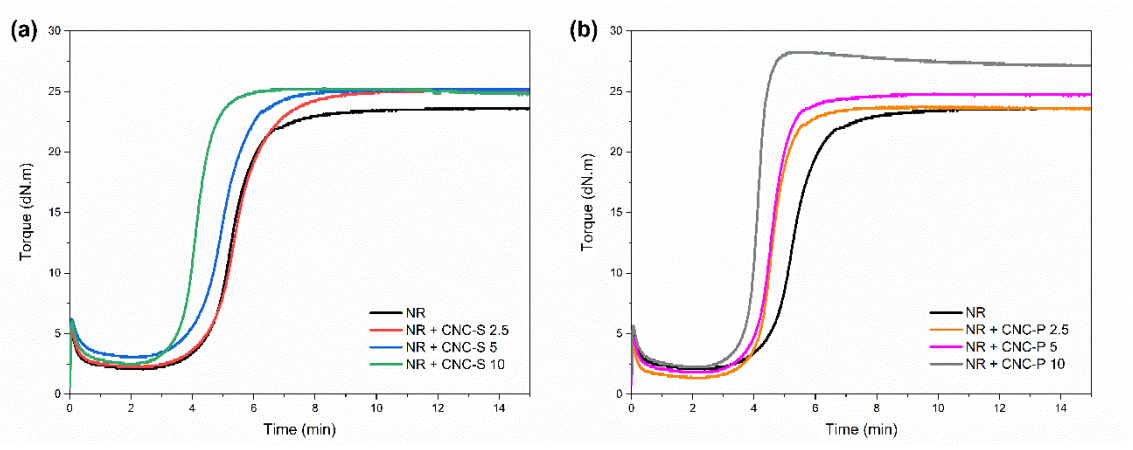

Fig. 6 Rheometric curves of (**a**) the NR compound without and with addition of CNCs extracted with H_2SO_4 (CNC-S) and (**b**) NR compound without and with addition of CNCs extracted with H_3PO_4 (CNC-P)

The vulcanization characteristics of the NR compound and composites, expressed in terms of maximum and minimum torque (M_H and M_L, respectively), pre-vulcanization time (scorch time, ts_2), optimal vulcanization time (t_{90}), torque variation (ΔM), and cure rate index (CRI), are summarized in Table 4.

Table 4 Vulcanization characteristics of the NR compound without and with CNC addition, at 160 °C.

Sample	M_L (dN.m)	M_H (dN.m)	ts_2 (min)	t_{90} (min)	ΔM^a (dN.m)	CRI[b] (min^{-1})
NR	2.0	23.6	4.32	6.48	21.6	46.3
NR + CNC-S 2.5	2.3	25.1	4.32	6.91	22.8	38.6
NR + CNC-S 5	3.1	25.2	3.91	6.15	22.1	44.6
NR + CNC-S 10	2.5	25.3	3.45	4.91	22.8	68.5
NR + CNC-P 2.5	1.4	23.7	3.97	5.39	22.4	70.4
NR + CNC-P 5	1.8	24.9	3.85	5.34	23.0	67.1
NR + CNC-P 10	2.3	28.2	3.57	4.48	26.0	109.9

[a] $\Delta M = M_H - M_L$

[b] CRI = Cure rate index = $100/(t_{90}-ts_2)$

The addition of filler to the NR compound results in an increase in the maximum torque. This behavior indicates an increase in the stiffness of the vulcanized compound owing to the restriction of the rubber chain mobility caused by the reinforcement addition (Lopattananon et al. 2006). Composites with 10 phr CNC-P exhibit the highest values of maximum torque and ΔM, which are related to the degree of intermolecular crosslinking.

The addition of CNCs reduced the optimal vulcanization time and increased the NR cure rates, particularly for samples with CNC-P. The longer vulcanization time of CNC-S composites might be due to the presence of sulfate groups on the surface of the crystals, which was not observed for CNC-P (Abraham et al. 2012).

The zinc and other crosslinking agents used to prepare the composites generate active sites for crosslinking in the NR backbone. Furthermore, they favor the breakdown of cellulose hydrogen bonds, which allows them to participate in the crosslinked network. The OH groups present in the cellulose chemical structure form a complex with zinc, and this process is discussed in the next section (3.7) (Abraham et al. 2012). Thus, it is suggested that compounds with CNC-P have more available OH groups and lower surface

charges compared to those with CNC-S, allowing the curing reactions to occur more rapidly. In addition, CNC-P particles have an average length 2.5 times longer than that of CNC-S particles and twice the aspect ratio, contributing to a stronger interaction between the filler and matrix phase.

Dispersion and network of CNC in NR nanocomposites

Fig. 7 shows the FEG-SEM images used to examine the dispersion of the CNC composites. These images were compared to those of NR compounds.

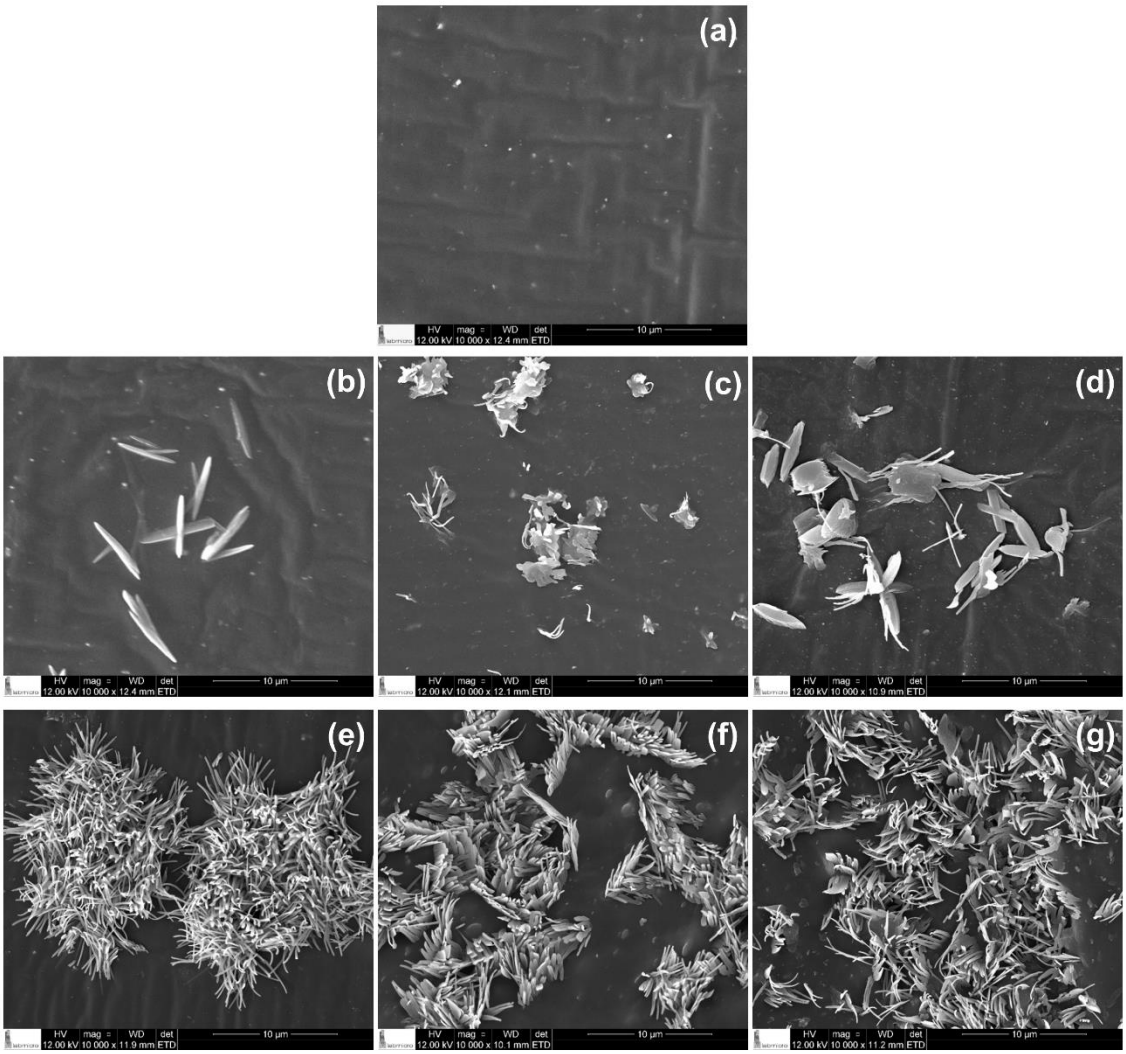

Fig. 7 SEM-FEG micrographs, at 10,000 times magnification, of the samples: NR **(a)**, NR + CNC-S 2.5 **(b)**, NR + CNC-S 5 **(c)**, NR + CNC-S 10 **(d)**, NR + CNC-P 2.5 **(e)**, NR + CNC-P 5 **(f)** and NR + CNC-P 10 **(g)**.

The morphologies of the composites differ from that of the NR compound. Composites with CNC-S present platelet-shaped particles (Fig. 7b, 7c, and 7d) and composites with CNC-P exhibit the form of needles (Fig. 7e, 7f, and 7 g). The filled and unfilled NR compounds are formed by dispersed phase elements, such as vulcanization additives, zinc oxide, and sulfur. The presence of vulcanization elements is more evident in the NR compound (Fig. 7a).

EDS spectra of unfilled and filled NR compounds are shown in Fig S-1 of the supplementary information. The results of the semi-quantitative EDS analysis confirm the highest zinc and sulfur content in the dispersed particles on the cryofractured surface of the NR compound. Considering the composites, the analysis indicates zinc and sulfur contents in the particles dispersed in the CNC-P composite lower than in those dispersed in the CNC-S composite. The CNC-P composites exhibit particle structures with flowers blooming at the surface of the compounds (Fig 7e, f, and g), unlike those observed in the CNC-S composites. Moreover, this structure probably results from the interaction between the Zn and OH groups present on the cellulose surface, or even a cluster of CNCs. The formation of these complexes is discussed in section (3.7).

Mechanical properties of the nanocomposites

Mechanical and crosslink density tests were performed on the NR compound and NR + CNC-S and NR + CNC-P composites, and the results are shown in Fig. 8.

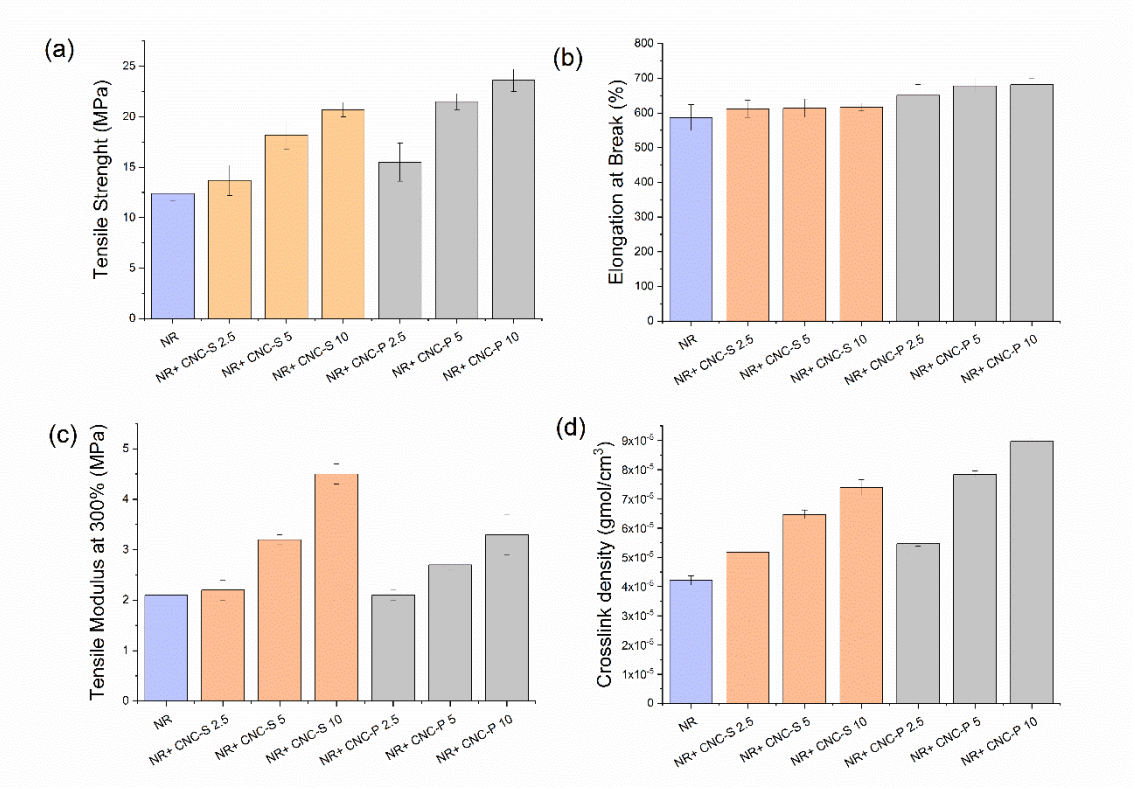

Fig. 8 Tensile tests of the NR compound and composites with different contents of CNC: tensile strength at break **(a)**, elongation at break **(b)**, modulus at 300% elongation **(c),** and crosslink density **(d)**.

Fig. 8 shows an increase in the values of all mechanical tensile properties of the composites produced from CNC-S as well as CNC-P, compared to the NR compound. The values of the tensile strength at break, elongation at break, and 300% modulus increased by 90 %, 16 %, and 52 %, respectively, for composites produced with 10 phr CNC-P, whereas for composites produced with 10 phr CNC-S, they increased by 68 %, 5 %, and 109 %, respectively, compared to the unfilled NR compound. The increase in tensile strength and modulus values as a function of the amount of the CNC added to the compound has already been reported (Visakh et al. 2012b; Abraham et al. 2013; Kumagai et al. 2019; Jardin et al. 2020).

Zinc oxide is a widely used vulcanizing agent in NR formulations, acting as an activator in this process. Combined with sulfur, the introduction of this compound as divalent metal ions allows reactions of oxidizing agents with alpha methylene carbon atoms or with polyisoprene double bonds (Stiehler and Wakelin 1947). These reactions result in an increase in the intermolecular forces in the NR compounds.

In this work, the introduction of Zn and vulcanizing agents with CNCs allowed the formation of Zn-cellulose complexes (Fig. 9) that allow enhancing the mechanical properties of the composites (Abraham et al. 2012; Thomas et al. 2015).

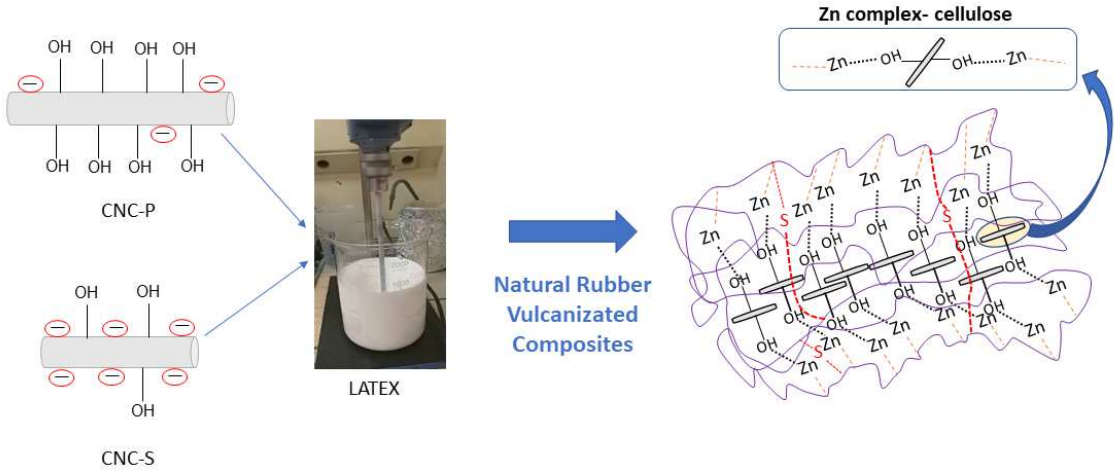

Fig. 9 Schematic formation of the Zn-cellulose complex in vulcanized NR compounds with CNC addition

Studies (Abraham et al. 2012, 2013) have shown that the introduction of crosslinking agents promotes sulfur reactions during vulcanization, allowing the breaking of the double bonds in the NR structure. The scission between the two active sites of NR and sulfur, which occurs during vulcanization, forms a crosslinking network. This crosslinking network forms with cellulose molecules, a stable complex with metal zinc, originating from zinc oxide. The addition of zinc oxide in the preparation of composites forms active sites in the NR by breaking the carbon double bonds and contributes to the deprotonation of cellulose which enables the breakdown of intramolecular and intermolecular hydrogen bonds by setting free OH groups on the cellulose surface. The alkaline latex medium and sonication process can also favor the scission of hydrogen bonds. The zinc reactions allow the OH groups to participate in the crosslinking network and the formation of a stable complex (Zn-cellulose) with the metal attached to the hydroxyl and carbon groups.

Therefore, the increase in the mechanical properties of NR compounds with the addition of CNCs is due to the synergistic effect of rubber-rubber, rubber-cellulose, Zn-cellulose, and cellulose-cellulose interactions (Fig. 9).

Furthermore, the high reinforcing effect of CNC-P can be attributed to the well-known phenomenon of percolation of high-aspect-ratio fillers, which form a more rigid continuous network of these nanoparticles compared to that formed by CNC-S. Furthermore, the mechanical properties of the composites can be attributed to the formation of a continuous cellulosic network when the threshold percolation is reached (Siqueira et al. 2010).

Although a decrease in elongation was expected (Abraham et al. 2012; Thomas et al. 2015) the results of the present study showed an increase, particularly for composites with CNC-P. An increase of 5% and 16% in the elongation of the composites prepared with 10 phr of CNC-S and CNC-P (Fig. 8b), respectively, can be attributed to an increase in the nanocellulose content, which decreases the micro spaces between the CNCs and the matrix. Moreover, the specific surface area of the reinforcement in contact with the matrix is larger for CNC-P compared to CNC-S, according to the nanoparticle dimensions reported in (Fig. 4); therefore, the elongation properties of the CNC-P composites are higher (Thomas et al. 2015).

The crosslink density of the NR compound and composites was evaluated, and the results presented in Fig. 8d show an increase with the addition of CNC to NR. The most pronounced result was observed for the composite with 10 phr of CNC-P. It is noteworthy that this sample exhibited the highest maximum torque and cure rate index values in the rheometric test and the highest modulus and tensile strength values in the mechanical test, compared to the NR compound and other composites.

Studies (Mathew et al. 2001; Arroyo et al. 2003; Cao et al. 2017; Correia and Valera 2019) showed similar results for rubber matrix composites and explained that this behavior may be related to the interfacial interaction between the filler and matrix, because strong filler-matrix interactions can hinder solvent permeation in the rubber matrix, reducing the volume of the absorbed solvent after the swelling test (Cao et al. 2017).

Conclusion

The influence of the introduction of CNCs on NR composites was investigated. The CNCs were extracted by hydrolysis using phosphoric (CNC-P) and sulfuric (CNC-S) acids. Compared to CNC-P, CNC-S had a lower thermal resistance because of the sulfate groups acting as catalysts for thermal degradation and the lowest aspect ratio.

Considering the properties of the composites, it was concluded that the addition of CNC-P to NR favored vulcanization. The CNC-P composites exhibited an increase in the maximum torque (M_H) and cure rate index values and a reduction in the optimal vulcanization time. This behavior might be due to the absence of phosphate groups on the surface of the nanocrystals and to the higher amount of OH groups on the cellulose surface compared to CNC-S.

Furthermore, the results of the mechanical tests confirmed that i) the CNC-P particles with longer lengths and higher aspect ratio, compared to those of CNC-S, resulted in the CNC-P composites having better mechanical properties; and ii) during the vulcanization process (crosslinking), metal Zn and cellulose nanoparticles formed a complex, increasing the adhesion between the CNCs and the elastomeric matrix. Moreover, an increase in the stiffness of the NR compound with CNC addition was confirmed through the increase in the elasticity modulus, enhancement in the tensile properties, and increase in the maximum torque values, according to the rheometric test. This behavior can be attributed to the strong charge-matrix interaction and the increase in the crosslink density, which reduces the mobility of the rubber molecules.

Therefore, CNCs are promising reinforcing agents for NR compounds, mainly in products such as rubber gloves or automotive components, which require the highest mechanical strength.

Acknowledgments

The authors are grateful to Dr. Marcio Yee from UNIFESP, and the Chemistry Department, USP. This research was supported by the LNNano – Brazilian Nanotechnology National Laboratory (CNPEM/MCTI) during the use of the AFM (proposal AFM-26460) open access facility.

Author contributions

All the authors contributed to the conception and design of the study. Material preparation, data collection, and analysis were performed by Carla Almeda Correia, Leticia Mota Oliveira, and Flavia Leticia Silva Freitas. The first draft of the manuscript was written by Flavia Leticia Silva Freitas and Carla Almeda Correa, and all the authors commented on and contributed to the previous versions of the manuscript. All authors have read and approved the final manuscript.

Founding

Financial support by Coordination for the Improvement of Higher Education Personnel (CAPES) from to the PNPD project no. 88887.373623/2019-00 and Proex number 0727/2020.

Data availability

All relevant data are within the manuscript and available from the corresponding author upon request.

Declarations

Conflict of interest

The authors declare that they do not have any conflict of interest about this manuscript.

Ethical approval

Not applicable.

Consent to participate

All authors were participated in this work.

Consent for publication

All authors agree to publish.

References

Abraham E, Deepa B, Pothan LA, et al (2013) Physicomechanical properties of nanocomposites based on cellulose nanofibre and natural rubber latex. Cellulose 20:417–427. https://doi.org/10.1007/s10570-012-9830-1

Abraham E, Elbi PA, Deepa B, et al (2012) X-ray diffraction and biodegradation analysis of green composites of natural rubber/nanocellulose. Polym Degrad Stab 97:2378–2387. https://doi.org/10.1016/j.polymdegradstab.2012.07.028

Ali SD, Imiete IE, Orlandi ME, et al (2020) Novel CNC/silica hybrid as potential reinforcing filler for natural rubber compounds. J Appl Polym Sci 137:48332. https://doi.org/10.1002/app.48332

609 Arroyo M, López-Manchado MA, Herrero B (2003) Organo-montmorillonite as
610 substitute of carbon black in natural rubber compounds. Polymer 44:2447–2453.
611 https://doi.org/10.1016/S0032-3861(03)00090-9
612 Camarero Espinosa S, Kuhnt T, Foster EJ, Weder C (2013) Isolation of thermally stable
613 cellulose nanocrystals by phosphoric acid hydrolysis. Biomacromolecules 14:1223–
614 1230. https://doi.org/10.1021/bm400219u
615 Cao L, Fu X, Xu C, et al (2017) High-performance natural rubber nanocomposites with
616 marine biomass (tunicate cellulose). Cellulose 24:2849–2860.
617 https://doi.org/10.1007/s10570-017-1293-y
618 Chawalitsakunchai W, Dittanet P, Loykulnunt S, et al (2019) Extraction of nanocellulose
619 from pineapple leaves by acid-hydrolysis and pressurized acid hydrolysis for
620 reinforcement in natural rubber composites. IOP Conf Ser Mater Sci Eng
621 526:012019. https://doi.org/10.1088/1757-899X/526/1/012019
622 Correia CA, Valera TS (2019) Cellulose Nanocrystals and Jute Fiber-reinforced Natural
623 Rubber Composites: Cure characteristics and mechanical properties. Mater Res
624 22:1–9. https://doi.org/10.1590/1980-5373-MR-2019-0192
625 Dittanet P, Somphol W, Lampang TN, et al (2019) Natural rubber reinforced by
626 nanocellulose extracted from dried rubber leaves. AIP Conf Proc 2083:030008.
627 https://doi.org/10.1063/1.5094318
628 Dufresne A (2012) Nanocellulose: From nature to high performance tailored materials.
629 De Gruyter, Berlin.
630 El Achaby M, Kassab Z, Barakat A, Aboulkas A (2018) Alfa fibers as viable sustainable
631 source for cellulose nanocrystals extraction: Application for improving the tensile
632 properties of biopolymer nanocomposite films. Ind Crops Prod 112:499–510.
633 https://doi.org/10.1016/j.indcrop.2017.12.049
634 Eyley S, Thielemans W (2014) Surface modification of cellulose nanocrystals. Nanoscale
635 6:7764–7779. https://doi.org/10.1039/c4nr01756k
636 Flory PJ, Rehner J (1943) Statistical mechanics of cross-linked polymer networks I.
637 Rubberlike elasticity. J Chem Phys 11:512–520. https://doi.org/10.1063/1.1723791
638 Formela K, Hejna A, Piszczyk Ł, et al (2016) Processing and structure–property
639 relationships of natural rubber/wheat bran biocomposites. Cellulose 23:3157–3175.
640 https://doi.org/10.1007/s10570-016-1020-0
641 Gan I, Chow WS (2019) Synthesis of phosphoric acid-treated sugarcane bagasse cellulose
642 nanocrystal and its thermal properties enhancement for poly(lactic acid)

643 nanocomposites. J Thermoplast Compos Mater 32:619–634.
644 https://doi.org/10.1177/0892705718772866
645 Gao TM, Huang MF, Xie RH, Chen HL (2013) Preparation and characterization of nano-
646 crystalline cellulose/natural rubber(NCC/NR) composites. Adv Mater Res 712–
647 715:111–114. https://doi.org/10.4028/www.scientific.net/AMR.712-715.111
648 Habibi Y, Lucia LA, Rojas OJ (2010) Cellulose nanocrystals: Chemistry, self-assembly,
649 and applications. Chem Rev 110:3479–3500. https://doi.org/10.1021/cr900339w
650 Huang L, Zhang X, Xu M, et al (2018) Preparation and mechanical properties of modified
651 nanocellulose/PLA composites from cassava residue. AIP Adv 8:025116.
652 https://doi.org/10.1063/1.5023278
653 Jacob M, Thomas S, Varughese KT (2004) Mechanical properties of sisal/oil palm hybrid
654 fiber reinforced natural rubber composites. Compos Sci Technol 64:955–965.
655 https://doi.org/10.1016/S0266-3538(03)00261-6
656 Jardin JM, Zhang Z, Hu G, et al (2020) Reinforcement of rubber nanocomposite thin
657 sheets by percolation of pristine cellulose nanocrystals. Int J Biol Macromol
658 152:428–436. https://doi.org/10.1016/j.ijbiomac.2020.02.303
659 Kargarzadeh H, Huang J, Lin N, et al (2018) Recent developments in nanocellulose-based
660 biodegradable polymers, thermoplastic polymers, and porous nanocomposites. Prog
661 Polym Sci 87:197–227. https://doi.org/10.1016/j.progpolymsci.2018.07.008
662 Kasyapi N, Chaudhary V, Bhowmick AK (2013) Bionanowhiskers from jute: preparation
663 and characterization. Carbohydr Polym 92:1116–23.
664 https://doi.org/10.1016/j.carbpol.2012.10.021
665 Kumagai A, Tajima N, Iwamoto S, et al (2019) Properties of natural rubber reinforced
666 with cellulose nanofibers based on fiber diameter distribution as estimated by
667 differential centrifugal sedimentation. Int J Biol Macromol 121:989–995.
668 https://doi.org/10.1016/j.ijbiomac.2018.10.090
669 Lavanya R, Natchimuthu N (2019) Decrystallization of cellulose under the influence of
670 elastomer-assisted mechanical and mechanochemical shear. Bull Mater Sci 42:168.
671 https://doi.org/10.1007/s12034-019-1852-y
672 Li MC, Wu Q, Song K, et al (2015) Cellulose Nanoparticles: Structure-Morphology-
673 Rheology Relationships. ACS Sustain Chem Eng 3:821–832.
674 https://doi.org/10.1021/acssuschemeng.5b00144
675 Lima MCFS, Zaida do Amparo S, Ribeiro H, et al (2016) Aqueous suspensions of carbon
676 black with ethylenediamine and polyacrylamide-modified surfaces: Applications for

chemically enhanced oil recovery. Carbon 109:290–299. https://doi.org/10.1016/j.carbon.2016.08.021

Lopattananon N, Panawarangkul K, Sahakaro K, Ellis B (2006) Performance of pineapple leaf fiber-natural rubber composites: The effect of fiber surface treatments. J Appl Polym Sci 102:1974–1984. https://doi.org/10.1002/app.24584

Lu Q, Lin W, Tang L, et al (2014) A mechanochemical approach to manufacturing bamboo cellulose nanocrystals. J Mater Sci 50:611–619. https://doi.org/10.1007/s10853-014-8620-6

Martins MA, Pessoa JDC, Gonçalves PS, et al (2008) Thermal and mechanical properties of the açaí fiber/natural rubber composites. J Mater Sci 43:6531–6538. https://doi.org/10.1007/s10853-008-2842-4

Martins MA, Teixeira EM, Corrêa AC, et al (2011) Extraction and characterization of cellulose whiskers from commercial cotton fibers. J Mater Sci 46:7858–7864. https://doi.org/10.1007/s10853-011-5767-2

Mathew AP, Packirisamy S, Radusch HJ, Thomas S (2001) Effect of initiating system, blend ratio and crosslink density on the mechanical properties and failure topography of nano-structured full-interpenetrating polymer networks from natural rubber and polystyrene. Eur Polym J 37:1921–1934. https://doi.org/10.1016/S0014-3057(01)00067-2

Moon RJ, Martini A, Nairn J, et al (2011) Cellulose nanomaterials review: Structure, properties and nanocomposites. Chem Soc Rev 40:3941–3994. https://doi.org/10.1039/c0cs00108b

Moonart U, Utara S (2019) Effect of surface treatments and filler loading on the properties of hemp fiber/natural rubber composites. Cellulose 26:7271–7295. https://doi.org/10.1007/s10570-019-02611-w

Nie J, Mou W, Ding J, Chen Y (2019) Bio-based epoxidized natural rubber/chitin nanocrystals composites: Self-healing and enhanced mechanical properties. Compos Part B Eng 172:152–160. https://doi.org/10.1016/j.compositesb.2019.04.035

Oliveira, MDM; Gonçalves ECP (2020) Impactos da SarS-CoV-2 na produção de borracha natural do Estado de São Paulo. Análises e Indicadores do Agronegócio. http://www.iea.sp.gov.br/ftpiea/AIA/AIA-67-2020.pdf . Accessed 04 April 2023.

Pantamanatsopa P, Ariyawiriyanan W, Meekeaw T, et al (2014) Effect of modified jute fiber on mechanical properties of Green Rubber composite. Energy Procedia 56:641–647. https://doi.org/10.1016/j.egypro.2014.07.203

711 Kanoth BP, Claudino M, Johansson M, et al (2015) Biocomposites from natural rubber:
712 Synergistic effects of functionalized cellulose nanocrystals as both reinforcing and
713 cross-linking agents via free-radical thiol-ene chemistry. ACS Appl Mater Interfaces
714 7:16303–16310. https://doi.org/10.1021/acsami.5b03115
715 Park S, Baker JO, Himmel ME, Parilla PA and Johnson DK (2010) Cellulose crystallinity
716 index: measurement techniques and their impact on interpreting cellulase
717 performance. Biotechnol Biofuels 3:2–10. https://doi.org/10.1186/1754-6834-3-10
718 Phanthong P, Reubroycharoen P, Hao X, et al (2018) Nanocellulose: Extraction and
719 application. Carbon Resour Convers 1:32–43.
720 https://doi.org/10.1016/j.crcon.2018.05.004
721 Ribeiro H, Da Silva WM, Neves JC, et al (2015) Multifunctional nanocomposites based
722 on tetraethylenepentamine-modified graphene oxide/epoxy. Polym Test 43:182–
723 192. https://doi.org/10.1016/j.polymertesting.2015.03.010
724 Roman M, Winter WT (2004) Effect of sulfate groups from sulfuric acid hydrolysis on
725 the thermal degradation behavior of bacterial cellulose. Biomacromolecules 5:1671–
726 1677. https://doi.org/10.1021/bm034519+
727 Shen XJ, Huang PL, Chen JH, et al (2017) Comparison of acid-hydrolyzed and TEMPO-
728 oxidized nanocellulose for reinforcing alginate fibers. BioResources 12:8180–8198.
729 https://doi.org/10.15376/biores.12.4.8180-8198
730 Silva MJ, Cena CR, Sanches AO, et al (2019) DBSA to improve the compatibility,
731 solubility, and infusibility of cellulose nanowhiskers modified by polyaniline in
732 reinforcing a natural rubber-based nanocomposite. Polym Bull 76:3517–3533.
733 https://doi.org/10.1007/s00289-018-2556-y
734 Siqueira G, Bras J, Dufresne A (2010) Cellulosic bionanocomposites: A review of
735 preparation, properties and applications. Polymers (Basel) 2:728–765.
736 https://doi.org/10.3390/polym2040728
737 Siqueira G, Tapin-Lingua S, Bras J, et al (2011) Mechanical properties of natural rubber
738 nanocomposites reinforced with cellulosic nanoparticles obtained from combined
739 mechanical shearing, and enzymatic and acid hydrolysis of sisal fibers. Cellulose
740 18:57–65. https://doi.org/10.1007/s10570-010-9463-1
741 Stiehler RD, Wakelin JH, (1947) Mechanism and Theory of Vulcanization. Ind Eng
742 Chem 39:1647–1654. https://doi.org/10.1021/ie50456a027
743 Tao H, Dufresne A, Lin N (2019) Double-network formation and mechanical
744 enhancement of reducing end-modified cellulose nanocrystals to the thermoplastic

elastomer based on click reaction and bulk cross-linking. Macromolecules 52:5894–5906. https://doi.org/10.1021/acs.macromol.9b01213

Thomas MG, Abraham E, Jyotishkumar P, et al (2015) Nanocelluloses from jute fibers and their nanocomposites with natural rubber: Preparation and characterization. Int J Biol Macromol 81:768–777. https://doi.org/10.1016/j.ijbiomac.2015.08.053

Tian M, Zhen X, Wang Z, et al (2017) Bioderived Rubber-Cellulose Nanocrystal Composites with Tunable Water-Responsive Adaptive Mechanical Behavior. ACS Appl Mater Interfaces 9:6482–6487. https://doi.org/10.1021/acsami.6b16308

Vanderfleet OM, Osorio DA, Cranston ED (2018) Optimization of cellulose nanocrystal length and surface charge density through phosphoric acid hydrolysis. Philos Trans R Soc A 376:20170041. https://doi.org/10.1098/rsta.2017.0041

Visakh PM, Thomas S, Oksman K, Mathew AP (2012a) Effect of cellulose nanofibers isolated from bamboo pulp residue on vulcanized natural rubber. BioRes 7:2156–2168. https://doi.org/10.15376/biores.7.2.2156-2168

Visakh PM, Thomas S, Oksman K, Mathew AP (2012b) Crosslinked natural rubber nanocomposites reinforced with cellulose whiskers isolated from bamboo waste: Processing and mechanical/thermal properties. Compos Part A Appl Sci Manuf 43:735–741. https://doi.org/10.1016/j.compositesa.2011.12.015

Wang J, Liu X, Jin T, et al (2019) Preparation of nanocellulose and its potential in reinforced composites: A review. J Biomater Sci Polym Ed 30:919–946. https://doi.org/10.1080/09205063.2019.1612726

Xie H, Du H, Yang X, Si C (2018) Recent Strategies in Preparation of Cellulose Nanocrystals and Cellulose Nanofibrils Derived from Raw Cellulose Materials. Int J Polym Sci 2018:. https://doi.org/10.1155/2018/7923068

Zhang C, Dan Y, Peng J, et al (2014) Thermal and mechanical properties of natural rubber composites reinforced with cellulose nanocrystals from southern pine. Adv Polym Technol 21448. https://doi.org/10.1002/adv.21448

(2018) Association of Natural Rubber Producing Countries (ANRPC). http:conab.gov.br. Accessed 10 Jan 2021

Supplementary Files

This is a list of supplementary files associated with this preprint. Click to download.

- GraphicalAbstractv.final.tif
- FigS1.pdf